Check for updates

Aurone-derived 1,2,3-triazoles as potential fluorescence molecules *in vitro*†

Daniel L. Bryant, [ID] [ab] Arjun Kafle,[b] Scott T. Handy, [ID] [b] Anthony L. Farone[a] and Justin M. Miller [ID] *[b]

Aurones are a class of well-studied natural compounds primarily responsible for the yellow pigment in flowering plants and have been shown to have fluorescent properties as well as beneficial biological effects. Traditionally, aurones can be easily synthesized through a Knoevenagel condensation of benzofuranones with arylaldehydes. Recently, Kafle *et al.* unexpectedly synthesized a new aurone derivative containing a 1,2,3-triazole within its backbone. Since, 1,2,3-triazole containing structures have been shown to be useful as fluorophores with large Stokes shifts, we hypothesized that these new aurone-derived triazole compounds (ATs) could be utilized as potential fluorophores. Here we describe a newly-synthesized fluorescent compound which has potential for use as a live-cell probe, having a large Stokes shift of 118.3 ± 1.01 nm in phosphate-buffered saline with the benefit of increased fluorescence in protic environments, which is uncommon in aurone-derived fluorophores.

Introduction

Aurones (2-benzylidene-1-benzofuran-3(2*H*)-one) are a class of naturally occurring flavonoid derivatives responsible for the pigments in some flowering plants, such as the yellow rocket snapdragon.[1] There has been a recent increase in the study of aurones due to their bioactivities;[2] including anti-inflammatory,[3–6] anti-microbial,[5,7,8] and anticancer[9–11] properties. In addition, there has been an interest in aurones as fluorescent markers due to their visible range excitation and emission spectra, tunable fluorescence properties, and their potential bioavailability.[12–14] Most notably, in 2011, Shanker and Dilek described four different aurones with a 4′ amine substitution on the benzylidene group (aminoaurones).[12] These aurones had increased Stokes shifts in more polar-protic solvents.[12] Two of the aminoaurones were shown to have increased emissions intensities in nonpolar solvents.[12] Other studies, both computational and experimental, have determined that the fluorescence spectra and Stokes shift of aurones are also dependent on side chain and solvent polarity.[13,14] For example, Espinosa-Bustos *et al.* observed increased emissions intensities in less polar solvents and that location of the sidechains on the benzylidene group of the aurone modulated the absorbance and emissions spectra, which supported the observations by Shanker and Dilek.[12,13] Xue *et al.* computationally examined the

aurones presented by Shanker and Dilek, and found that the increased Stokes shifts and red-shifted emissions were due primarily to intramolecular charge transfer.[14] Muñoz-Becerra *et al.* in 2019 described computationally how the addition of a polar side chain on the 4 carbon of the benzofuranone backbone led to an increased Stokes shifts as well as red-shifted absorbance and emissions spectra.[15]

Aurones have also been examined for potential as fluorescent sensors. Starting in 2013, Chen and associates synthesized multiple aurone-based sensors for cyanide.[16–18] In 2018, Zhang *et al.* described a membrane permeable aurone based sensor for Hg^{2+}.[19] Most recently, Kafle *et al.* in 2020 developed an aurone-derived sensor for hydrogen sulfide.[20] Though the potential for aurones as bioavailable fluorescent molecules has been reported, aurones traditionally only fluoresce in non-polar solvents and are quenched in aqueous environments.[12,13,20] Kafle *et al.* were able to bypass the quenching effect of aqueous environments through the use of hexadecyl-trimethylammonium bromide (CTAB).[20]

Finding new methods of aurone synthesis has been an area of active research for many years. Two common methods of aurone synthesis were described by Geissman and Harborne in 1955 where they used a condensation reaction between a coumaranone and various aldehydes,[21] and by Varma and Varma in 1992 in which they used an alumina catalyzed reaction of benzofuranones with arylaldehydes.[22] Alternatively, others have utilized palladium and formic acid,[23] silver nitrate,[24] gold,[25] or choline chloride and urea[26] in various condensation and cyclization approaches to the aurone skeleton. In the course of an effort to install an azido group on an intact aurone system, Kafle

[a]Department of Biology, Middle Tennessee State University, 1301 E Main St., Murfreesboro 37132, Tennessee, USA

[b]Department of Chemistry, Middle Tennessee State University, 1301 E Main St., Murfreesboro 37132, Tennessee, USA. E-mail: Justin.Miller@mtsu.edu
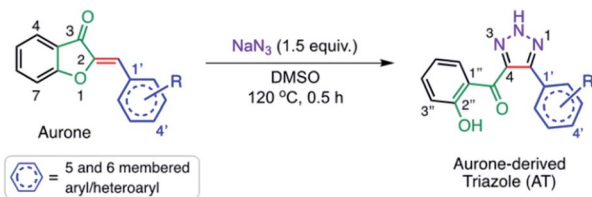
Fig. 1 Synthesis of aurone-derived triazoles.

et al. noted instead the synthesis of a new class of aurone-derived salicyl substituted 1,2,3-triazole (AT) (Fig. 1).[27]

1,2,3-Triazoles have also been shown to possess fluorescent properties.[28–30] In 2015, Ghosh *et al.* described a "click" synthesized 1,2,3-triazole which showed fluorescence in the presence of a fluoride ion.[28] In 2018, Meisner *et al.* established that 1,2,3-triazole containing compounds have larger Stokes shifts with their fluorescent properties affected by the triazole substitution and the ability to form intramolecular hydrogen bonds.[30] Unlike the other 1,2,3-triazoles, the aurone-derived ATs incorporate a salicylic group substituted at C4 on the triazole ring (Fig. 1). With this in mind, it was thought that ATs would have potential as fluorescent compounds. It was hypothesized that 1,2,3-triazoles derived from aurones would have fluorescent properties similar to both triazoles and aurones. Here, we describe ATs with increased fluorescence in polar protic aqueous environments, allowing for increased fluorescence in cellular environments with marked potential as a biologically relevant fluorescent probe.

Materials and methods

All the reactions and handling of the chemicals were done under an air atmosphere using ACS-grade reagents. Organic solvents were directly employed without further purification. ^{1}H and ^{13}C NMR of all the compounds were recorded on JEOL AS (500 and 125 MHz respectively), using CDCl$_3$, DMSO-D_6, or acetone-D_6 as a standard reference (Fig. S1†).[31] Chemical shifts and the coupling constants (*J*) for ^{1}H and ^{13}C NMR are reported in parts per million (ppm) and in hertz (Hz), respectively. The following conventions are used for multiplicities: s, singlet; d, doublet; t, triplet; m, multiplet; dd, doublet of doublet; tt, triplet of triplet; dt, doublet of triplet; ddd, doublet of doublets of doublets; br, broad. All high-resolution mass spectra were acquired on a Waters Synapt HDMS QToF with Ion Mobility. Reactions were monitored by Thin Layer Chromatography (TLC) on silica-coated plates using short-wavelength (254 nm) UV light. All extracts were concentrated under reduced pressure using Buchi Rotary Evaporator. The compounds were purified by flash silica gel (32–64 μm) column chromatography.

General procedure for the synthesis of aurone-derived triazoles (AT1–AT5)

The aurones and the corresponding triazoles, **AT1–AT5** (structures in Fig. S2†) were synthesized and characterized based on the literature.[21,27] The characterization data for **AT2** and **AT5** are provided below. Following preparation of the aurone,[21] 0.50 mmol of aurone was mixed with 0.75 mmol (1.5 eq.) of sodium azide (NaN$_3$) using 1.5 mL DMSO in a 3-dram glass vial and heated at 120 °C for 30 min (unless otherwise specified) in a sand bath. The progress of the reaction was monitored by TLC. After the completion of the reaction, the reaction mixture was cooled to room temperature and transferred to a 50 mL centrifuge tube. It was then diluted with DI water and extracted several times with ethyl acetate (150 mL). Next, the obtained organic fraction was washed with DI water followed by brine. Finally, the organic fraction was dried over anhydrous MgSO$_4$ and concentrated *in vacuo* to obtain the crude product, which was purified by flash column chromatography using mixtures of hexane and ethyl acetate (20–50% EtOAc/hexane) to afford the desired triazole.

(5-(5′-Bromothiophen-2′-yl)-2H-1,2,3-triazol-4-yl)(2″-hydroxyphenyl)methanone (AT2). Reaction scale: 0.325 mmol (99.8 mg); purified by column chromatography (20% EtOAc/hexane); yield: 31.6% (36 mg); orange solid, mp: 159.5–162 °C; ^{1}H NMR (500 MHz, chloroform-D_6) δ 12.04 (s, 1H), 11.82 (s, 1H), 8.21 (dd, *J* = 8.1, 1.4 Hz, 1H), 7.61 (d, *J* = 3.9 Hz 1H), 7.59–7.51 (m, 1H), 7.11–7.04 (m, 2H), 6.94 (t, *J* = 7.7 Hz, 1H). ^{13}C NMR (125 MHz, chloroform-D_6) δ 191.3, 163.9, 137.4, 133.7, 130.7, 129.7, 119.5, 119.3, 118.58, 115.9, 110.5, 109.9. IR (neat) 3177, 2954, 1721, 1628, 1603, 1482, 1257, 909, 747 cm^{-1}. HRMS: calcd for C$_{13}$H$_8$BrN$_3$O$_2$S 348.9520, observed 348.9518.

(5-(4′-Acetamidophenyl)-2H-1,2,3-triazol-4-yl)(2″-hydroxyphenyl)methanone (AT5). Reaction scale: 0.716 mmol (200 mg); reaction time = 2 h; purified by column chromatography (70% EtOAc/hexane); yield: 40% (92 mg); yellow solid, mp = 216–220 °C. ^{1}H NMR (300 MHz, DMSO-D_6) δ 11.07 (s, 1H), 10.13 (s, 1H), 7.89–7.82 (m, 1H) (br), 7.68 (s, 4H), 7.50 (t, *J* = 7.7 Hz, 1H), 6.98–6.91 (m, 2H), 2.07 (s, 3H). ^{13}C NMR (125 MHz, DMSO-D_6) δ 190.9, 168.5, 159.9, 140.2, 135.2, 132.2, 128.9, 122.7, 118.9, 118.6, 117.2, 24.0. IR (neat) 3330, 1655, 1581, 1462, 1317, 1251, 1158, 989, 922, 750 cm^{-1}. HRMS: calcd for C$_{17}$H$_{14}$N$_4$O$_3$ 322.1069, observed 322.1973.

General protocols

All ATs were reconstituted from a purified powder at 100 mM in 100% dimethyl sulfoxide (DMSO; Fisher Scientific, MA; Cat#: D128-500/MP Biomedicals; Cat#: 196 055). In all experiments the ATs were diluted to 100 μM in the indicated solution with 0.1% (v/v) DMSO as a cosolvent. To account for DMSO as a cosolvent, all experiments were carried out with 0.1% (v/v) DMSO as a vehicle control. For experiments measuring fluorescence spectra, the absorbance and emissions of the vehicle control were subtracted as a background.

Cell culture

Raw 264.7 murine macrophage-like cells (ATCC Cat#: TIB-71) and HeLa cells (ATCC Cat#: CCL-2) were cultured in either Dulbecco's modification of Eagle's Medium (DMEM; Corning, NY; Cat#: 10-013-CV) or Roswell Park Memorial Institute 1640 medium (RPMI; Fisher Scientific, MA; Cat#: 11 875 093), respectively. Both media were supplemented with 10% heat-

inactivated fetal bovine serum and 100 units/mL penicillin/streptomycin cocktail (Fisher Scientific, MA; Cat#: 15-140-122). The cells were grown in a humidified incubator at 37 °C with 5% CO_2 and passaged prior to reaching 90% confluency every 3–5 days. All cell culture experiments were incubated in this manner unless otherwise stated.

Cytotoxicity assay

Cytotoxicity of each AT was determined using the PrestoBlue cell viability assay (Invitrogen, CA; Cat# A13262). RAW 264.7 cells, or HeLa cells, were seeded at a density of 5×10^4 cells per well, or 1×10^4 cells per well, respectively, in a sterile 96-well plate and allowed to attach overnight. The cells were washed with 1X phosphate-buffered saline (PBS; Gibco – ThermoFisher Scientific, MA; Cat#: 10 010023), then treated with 100 μM of each AT, or 0.1% (v/v) DMSO as a vehicle control, for 24 h. Immediately following the treatment, the cells were washed with PBS, and medium containing 1X PrestoBlue was added to the cells for one hour. The absorbance at 570 nm was recorded, and the absorbance at 600 nm was subtracted according to the manufacturer's protocol. The data is presented as a percentage to the average absorbance of the untreated wells for each plate ± SEM.

Confocal microscopy

Live cell imaging. RAW 264.7 cells or HeLa cells were seeded at 1×10^6 cells per well and 6×10^5 cells per well respectively in 35 mm culture dishes with a glass coverslip inlay (Cellvis, Burlington, Canada; Cat#: D35-14-1.5 N) and allowed to attach overnight. The cells were washed 16–18 h post seeding and treated with 100 μM of the indicated AT for an additional 24 h. The cells were imaged post 24 h on a Zeiss LSM 700 confocal microscope. In experiments comparing the different fluorescent properties of each, the ATs were excited with a 405 nm and 555 nm lasers (gain = 650; pinhole 0.92 AU) simultaneously, with detection wavelengths of 300–483 nm and 560–800 nm, respectively, then excited with a 455 nm laser (gain = 650; pinhole = 0.9 AU) with a detection wavelength of 300–598 nm. For experiments where AT5 was imaged alone, it was excited with a 405 nm laser (gain = 650) with a detection wavelength of 300–598 nm. For time-course experiments, RAW 264.7 cells were washed with PBS 16 h post seeding and 1 mL of medium was added. Cells were then transferred to a Zeiss LSM 700 confocal microscope with a 37 °C, 5% CO_2 life support chamber for at least 30 min prior to imaging. The cells were treated with 1 mL of 200 μM AT5 for a final concentration of 100 μM, and immediately imaged. The cells were then imaged immediately as well as every 15 min post treatment for 23 h and 45 min using a 405 nm laser (gain = 600; pinhole = 1.05 AU) with a detection wavelength of 300–584 nm. The cells analyzed were chosen due to survival and tracking until the end of the experiment. Brightness of each image was increased equally in each figure post analysis for clarity.

Fixed cell imaging. RAW 264.7 cells were seeded as described. The following day, the cells were washed with PBS and fixed in 1 mL of 4.0% (v/v) formaldehyde (Fisher Scientific, MA; Cat#: F75P-4) for 10 min. The cells were washed, and the membranes of the cells were permeabilized with 1 mL of 0.1% (v/v) Triton X-100 (Sigma Aldrich, MO; Cat#: T8787) in PBS for 5 min. Excess Triton was removed, and the cells were then stained with 500 μM AT5 or 0.5% (v/v) DMSO as a vehicle control for 30 min. The cells were then washed two more times with PBS to remove excess AT5 and imaged on the Zeiss LSM 700 confocal microscope using a 405 nm laser (gain 650; pinhole = 1.27 AU) with a detection wavelength of 300–584 nm. The raw fluorescence intensity of each cell was determined by measuring the intensity of the signal in the. CZI file using FIJI.[32] The data is presented as a background corrected mean signal intensity for unit area (pixel) of each cell.

Absorbance and emissions microplate procedure

Absorbance and emissions spectra for AT5 at varying concentrations were determined by mixing 400 μM of AT5 or 0.4% (v/v) DMSO in PBS (Growcells, CA; Cat#: MRFG-6235) in a 96-deep-well plate (ThermoFisher Scientific, MA; Cat#: 260 251). AT5, or vehicle, was then diluted serially to 6.25 μM in PBS. 100 μL of each concentration was transferred to a UV/Vis 96-well microplates (Fisher Scientific, MA; Cat#: 21-377-832) in triplicate for three independent replicates ($n = 9$). Both absorbance and emissions spectra were measured using a CLARIOstar microplate reader (BMG-Labtech, Germany). Absorbance was measured at each wavelength from 220–1000 nm using the average of 5 flashes per well. The emissions spectra from 350–621 nm (emission bandwidth of 14 nm) were measured using an excitation wavelength of 320 nm (excitation bandwidth of 12 nm) at a gain of 857 and a focal length height of 5 mm using the top optic. Absorbance and emissions spectra for the vehicle at each concentration were subtracted as background.

Solvent polarity

To determine the effect of solvent polarity, 100 mM AT5 in DMSO was mixed with 1 mL of each indicated solvent to a final concentration of 100 μM. Peak excitation was determined by screening emissions of AT5 at 330 nm on a Hitachi F-4500 fluorescence spectrophotometer. Optimal excitation wavelength was determined for each compound by systematically varying excitation wavelength in 0.1 nm increments until the emissions maximum was observed. Emissions spectra were then recorded using the peak excitation for each solvent. Emissions data for 0.1% (v/v) DMSO was gathered for each solvent and subtracted as a baseline.

pH sensitivity

The effect of changes in pH of 1X PBS was determined by using 10X PBS (Growcells CA, Cat#: MRFG-6235) diluted with either hydrochloric acid or sodium hydroxide and water to 1X PBS. The acidic or basic 1X PBS was then used to change the pH of 1X PBS to either 5.0, 6.0, 7.0, 7.4, 8.0, 9.0, or 10.0. AT5 was then diluted to 100 μM in the PBS at each pH. Each well was mixed in a 96-deep-well plate and 100 μL of each was loaded into UV/Vis 96-well microplates (Fisher Scientific, MA; Cat#: 21-377-832) in triplicate for three independent replicates. Emissions were measured using a CLARIOstar microplate reader as previously

described. Emissions spectra for 0.1% (v/v) DMSO at each pH was subtracted as background.

Detergent interactions

To determine the effect of different detergents on **AT5**, 100 mM of **AT5** was diluted to 100 μM in the indicated concentrations of either CTAB (Sigma Aldrich, MO; Cat#: H 6269; CMC = 0.9 mM[33]), SDS (Fisher Scientific, MA; Cat#: 166-100; CMC ≈ 8 mM[34,35]), Triton X-100 (Fisher Scientific, MA; Cat#: BP151-500; CMC = 0.18–0.24 mM[36–39]), or Tween 20 (Fisher Scientific, MA; Cat#: BP337-100; CMC ≈ 0.050–0.057 mM[37,40]), as well as PBS pH 7.4 (Growcells, CA; Cat#: MRFG-6235) and 18 mΩ H₂O. To determine the correct order of mixing, 100 mM **AT5** was diluted to 100 μM in PBS and H₂O either 30 min before or after the addition of Triton X-100 at a final indicated concentration and mixed *via* pipetting. To create a broad range of emissions for **AT5**, 100 μM of **AT5** in PBS was mixed with the indicated ratios of both Triton X-100 and SDS to a final detergent concentration of 100 mM. Absorbance and emissions spectra were measured for each well using a CLARIOstar microplate reader as previously mentioned.

Results and discussion

Five ATs; **AT1**, **AT2**, **AT3**, **AT4**, and **AT5** were initially screened for potential fluorescence *in vitro* using confocal microscopy (Fig. 2). RAW 264.7 cells were treated with the various ATs for 24 h prior to imaging. These results demonstrated that cells treated with 100 μM of either **AT2** or **AT5** showed notable amounts of fluorescence (Fig. 2A and B). **AT5** exhibited emissions when excited by the 405 nm (blue) laser while **AT2** did so when excited using both the 488 nm (green) and 555 nm (red) lasers, but not the 405 nm laser (Fig. 2A, B, and S2†). The observation of minor **AT5** emissions intensities, relative to DMSO, in the green- and red-channels may be the consequence of crosstalk between channels based on microscope experimental parameters. This conclusion is supported by the lack of **AT5** absorbance at these wavelengths as noted in Fig. 5 below. In addition to their differences in fluorescence, both ATs seemed to localize to different areas within the cell; although, from the data collected it is difficult to determine the exact locations of each fluorophore (Fig. 2C). Of these ATs only **AT5** showed no statistically significant cytotoxic effect on RAW 264.7 murine macrophage-like cells after 24 h, with an average of 90.7 ± 11.3% cell viability (Fig. 3A). It should be noted that all examined ATs were cytotoxic to HeLa cells after 24 h (Fig. 3B). **AT5** was the least cytotoxic with an average of 73.5 ± 16.3% cell viability (Fig. 3B). This apparent lower cytotoxicity may be due to the large methyl acetamide side chain of **AT5** compared to the side chains of **AT1–4** (Fig. 2 and S2†). Although **AT2** showed potential as a fluorescent probe, the cytotoxicity prohibited its use in live-cell imaging experiments. Additionally, preliminary
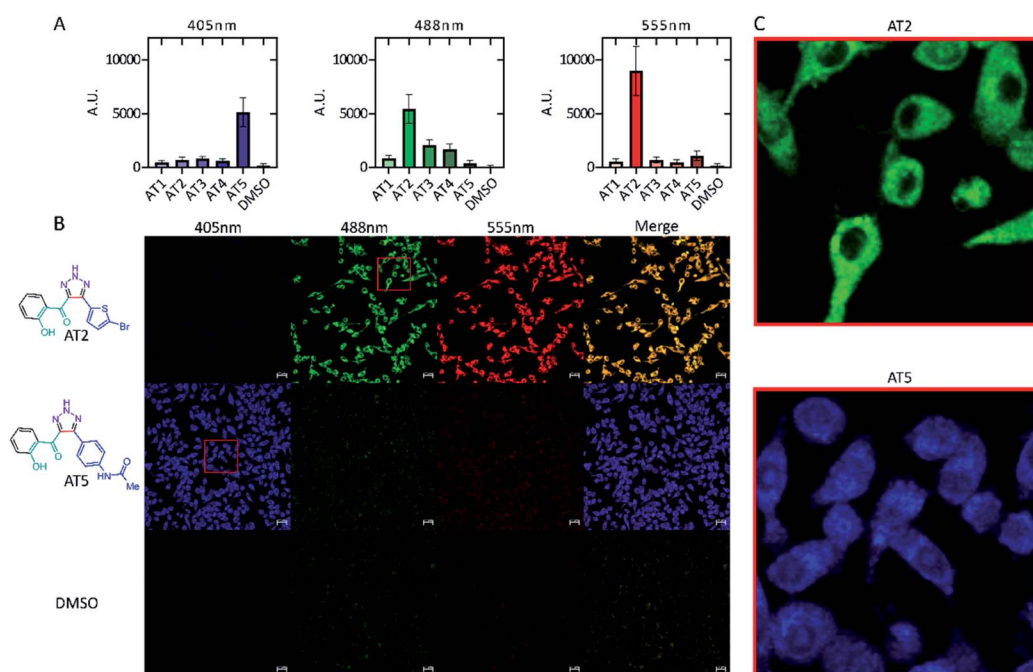

Fig. 2 Fluorescence intensity of ATs *in vitro*. RAW 264.7 murine macrophages were incubated for 24 h with 100 μM of the indicated compound. Cells were imaged using a Zeiss LSM 700 confocal microscope with excitation wavelength indicated as 405 nm, 488 nm, or 555 nm. Signal intensity for cells for each laser were measured using FIJI and standardized to the unit area of each cell. Background in each image was subtracted from each measurement. Values where the fluorescence intensity of the cell was less than the background (negative values) were set to zero. (A) Mean emission intensity ± SD *n* = 150 for each compound. Cells were sampled at random from various fields using the transmitted light image to avoid bias (not shown) across three, independent biological replicates. Emission intensities were determined as a quantification of (B) (and Fig. S2†) showing the fluorescence of each compound *in vitro* for each specific laser. Scale bars are 20 μm. (C) Enlarged regions of each photo showing distribution of ATs *in vitro*. Brightness across all images was adjusted equally post analysis.
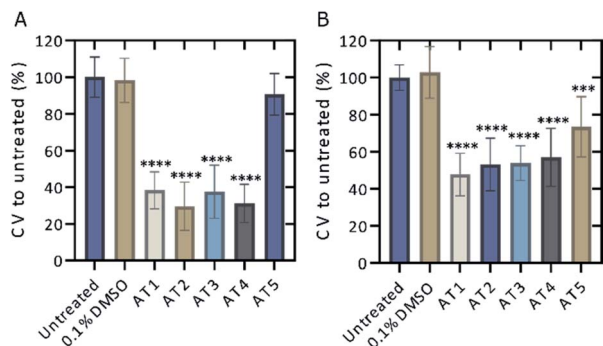
Fig. 3 Cell viability of (A). RAW 264.7 cells and (B). HeLa cells after 24 h treatment with each compound. PrestoBlue and media (1 : 1 ratio) were added to either RAW 264.7 cells or HeLa cells for 1 h post treatment and incubated at 37 °C. Values are shown as the ratio of the difference of absorbance at 570 nm signal and the 600 nm background for each sample to the difference in absorbances for the average of the untreated means ± SD. Each assay was performed in triplicate for three, independent biological replicates, $n = 9$. Statistical significance was determined using a Brown–Forsythe and Welch's ANOVA. ***$p < 0.001$, ****$p < 0.0001$.

characterization of **AT2** showed little fluorescence in PBS, DMSO, and cyclohexane (data not shown). Though this may imply **AT2** is interacting with something within the cell to increase its fluorescence. Further research outside the scope of this paper is needed to fully understand this phenomenon. Due to the observed fluorescence and lack of cytotoxicity, **AT5** was further pursued for additional characterization.

To determine whether the fluorescence activity of **AT5** was only visible in RAW 264.7 cells, both RAW 264.7 cells and HeLa cells were incubated with 100 μM **AT5** for 24 h at 37 °C in a 5% CO_2 incubator and imaged using the Zeiss LSM 700 confocal microscope. We found that although there is a slight difference

in the fluorescent intensity of **AT5** in HeLa and RAW 264.7 cells (comparison not shown), **AT5** could indeed be used as a live-cell probe in different cell lines (Fig. 4A and B). To determine the timeframe required for use with live cells, RAW 264.7 cells were treated with 100 μM **AT5** at 37 °C in 5% CO_2 and imaged every 15 min for approximately 24 hours (Fig. 4C). Though fluorescence consistently increased, changes in fluorescence increased approximately 4 h post-treatment, at which point the fluorescence intensity seemed to increase at a greater rate for the remainder of the experiment (Fig. 4C). Additionally, fluorescence intensity of **AT5** in RAW 264.7 cells never plateaued indicating the potential for increased fluorescence at time points of 24 h or later (Fig. 4C). There was observable cell death at time points approaching 24 h, which is potentially due to prolonged exposure to the 405 nm laser because in fields adjacent to the final images of this experiment, there was little to no observable cell death (images not shown). This is supported by the previously mentioned cell viability experiments (Fig. 3). In addition to acting as fluorophore in live cells, **AT5** was able to stain fixed and permeabilized RAW 264.7 cells (Fig. S3†) further indicating its applicability. In many images, **AT5** can be seen inside both RAW 264.7 cells and HeLa cells, though it does not seem to be ubiquitous throughout the cell (Fig. 2B, C, 4A, and S2†). It is possible that **AT5** is not simply sequestered, but rather interacting with cellular components. Further research is necessary to validate this idea. Our initial results indicate that pH may also play a role in fluorescence since we observed a slight reduction in emissions of **AT5** in PBS with a pH ≤ 6 (Fig. S4†).

Changes in AT5 fluorescence due to solvent polarity

Solvent polarity has been previously reported to affect the emissions of aurones and their derivatives, showing a trend for increased emissions as polarity decreased.[12,13] It was
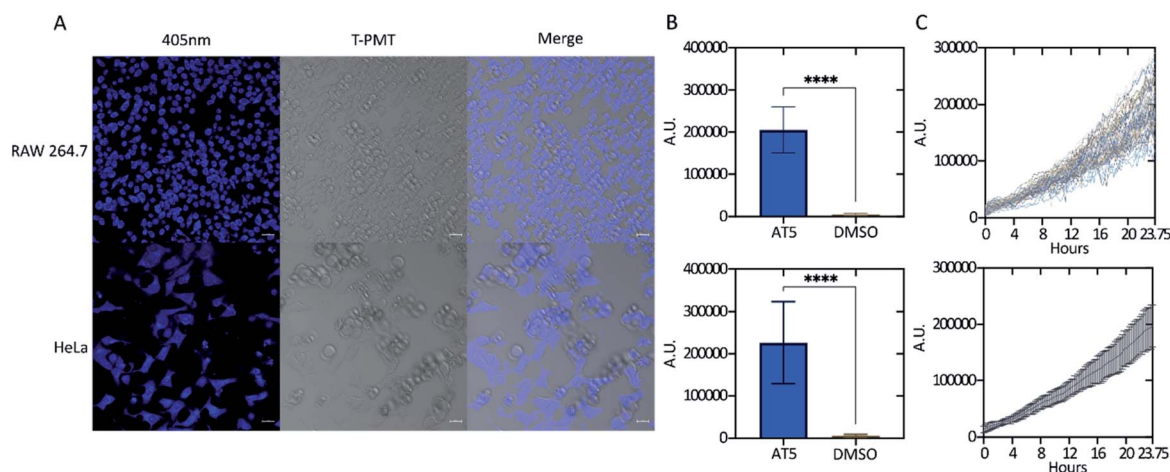

Fig. 4 (A) Fluorescence in RAW 264.7 cells and HeLa cells. Brightness across all images was adjusted equally post data analysis. (B) Quantification of (A) shown as the mean fluorescent signal per unit area ± SD in RAW cells (top) and in HeLa cells (bottom) treated with 100 μM AT5 or 0.1% (v/v) DMSO for 24 h, $n = 300$ cells over 3 independent replicates. Statistical analyses were done using a using a two-tailed t-test with a Welch's correction, ****$p < 0.0001$. Values where the fluorescence intensity of the cell was less than the background (negative values) were set to zero. (C) Fluorescence signal per unit area in RAW 264.7 cells over time. Images were taken every 15 min for 23.75 h. Data for each individual cell is shown (top) along with the mean ± SD (bottom). $n = 60$ cells across three independent biological replicates.
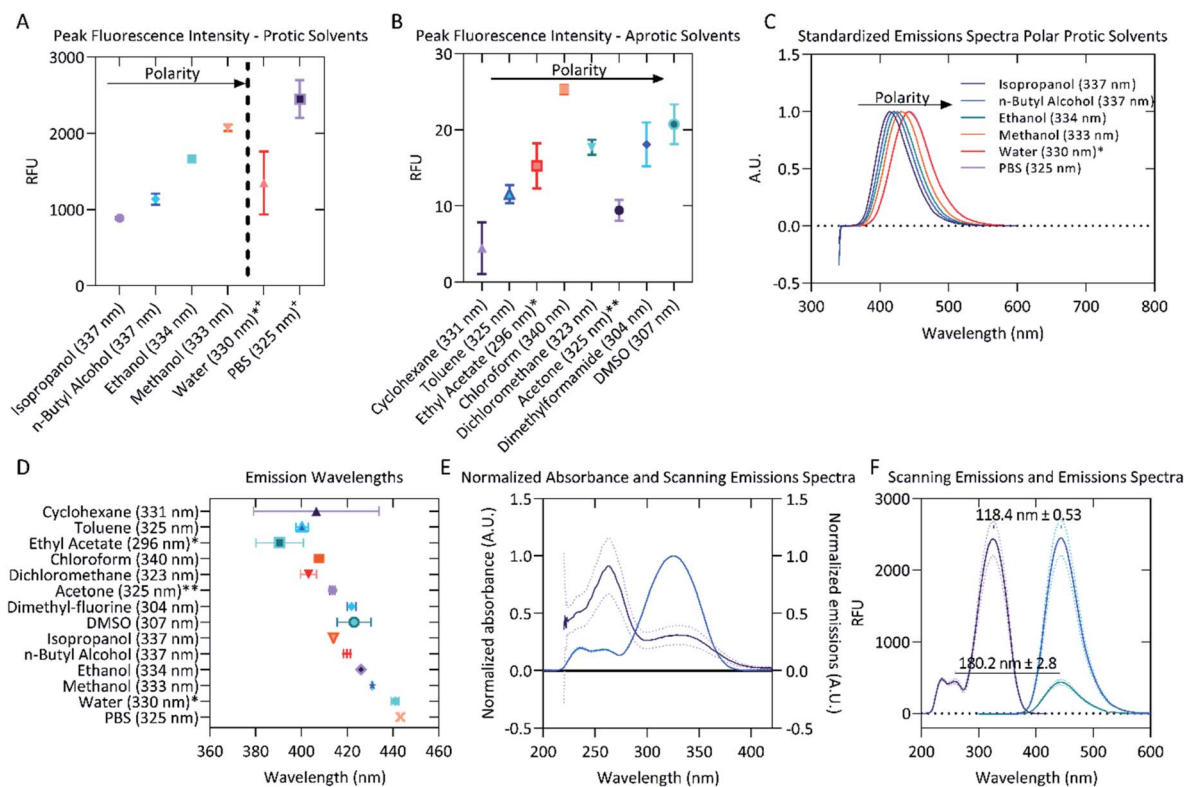
Fig. 5 Fluorescent properties of 100 μM **AT5** in different solvents. (A) Emission intensities of **AT5** in various protic solvents organized by increasing polarity. Excitation wavelengths (in parenthesis) were determined using the scanning emissions spectra. (B) Emission intensities of **AT5** in various aprotic solvents organized by increasing polarity. Excitation wavelengths (in parenthesis) were determined using the scanning emissions spectra. (C) Red-shift in emission spectra for protic solvents. The mean emissions spectra for each solvent were standardized, 1 being the highest emission intensity and 0 set to 0 emissions. Excitation wavelengths (in parenthesis) were determined using the scanning emissions spectra. (D) Peak emission wavelengths for **AT5** in various solvents. Excitation wavelengths (in parenthesis) were determined using the scanning emissions spectra. (E) Normalized absorbance (solid purple line) and normalized scanning emission (solid blue line) spectra $\pm$ SD, $n = 9$ across three independent replicates measured using a CLARIOstar microplate reader. Absorbance and scanning emissions spectra for wavelengths > 420 nm not shown. (F) Scanning emissions spectra (solid purple line) and emission (solid blue line) spectra of PBS $\pm$ SD measured using the spectrophotometer, $n = 3$. Excitation wavelengths (in parenthesis) were determined using the scanning emissions spectra. For all panels (A–F), each emission spectra for the various solvents were measured and blank corrected using 0.1% (v/v) DMSO as a vehicle background. Peak emissions and peak emission wavelengths were determined as $n = 3$ independent replicates for the indicated excitation wavelength (in parenthesis) with mean values represented. Vertical lines represented standard deviation calculated for each set of measurements. *Low solubility. **Negative values for one replicate led to only using an $n = 2$. [+]Aqueous solvents not statistically different due to high variability. [0]Polarity data not known for PBS. [1]Polarity based on the relative normalized E_T (30) [E_T^N] polarity.[41]

hypothesized that polarity may influence the fluorescent properties of **AT5** as well. To test this, **AT5** was dissolved to a concentration of 100 μM in various solvents. Each solvent was ranked according to the relative normalized molar electronic transition energies of pyridium *N*-phenolate betaine dye 36 (E_T (30)) values (E_T^N) on a scale between tetramethylsilane (TMS; 0.00) and water (1.00).[41,42] Surprisingly, it was found that the fluorescence of **AT5** increased in polar-protic environments, with the greatest fluorescence occurring in PBS (Fig. 5A). Indeed, even the weakest fluorescence in a polar-protic solvent (isopropanol, 889.1 $\pm$ 10.96 [SD] RFU) exhibited more than 35-fold stronger emissions ($p < 0.0001$; Unpaired two-tailed *t*-test with a Welch's correction) compared to chloroform (25.3 $\pm$ 0.86 [SD] RFU) which had the strongest emissions of both the polar-aprotic and non-polar solvents (Fig. 5A). Given that the E_T (30) scale is well known to be highly sensitive to hydrogen-bonding, these results were also examined in the context of the pi* scale,

which reflects more general solvent polarity.[42–44] There was effectively no correlation of fluorescence results with the pi* scale indicating that hydrogen-bonding is indeed the dominant feature influencing fluorescence intensity, although it should be noted that no attempt was made to ensure anhydrous conditions during fluorescence measurements, so the influence of residual water in the solvents or on the cuvettes cannot be ruled out.

Water is the most polar-protic solvent on this scale, so it was expected that water would cause **AT5** to have the highest fluorescence emissions, but due to the low solubility of **AT5** in water, it was unable to go fully into solution potentially limiting its detectable fluorescence. The data also suggests that polarity in aprotic solvents has little to no effect on the fluorescence emissions of **AT5**, but rather is dependent on the protic nature of the solvent (Fig. 5A and B and Table 1). This suggests a potential use of **AT5** in selective fluorescence visualization

Table 1 Stokes shift and peak emissions of AT5 in various solvents. Emission spectra for AT5 in various solvents was measured and blank corrected using 0.1% (v/v) DMSO as a vehicle background. Peak emissions and peak emission wavelengths were determined as $n = 3$ independent replicates for the indicated excitation wavelength. Stokes shift was determined as the difference between the excitation wavelength and the peak emissions wavelength, $n = 3$ *Low solubility. **Negative values for one replicate led to only using an $n = 2$. [+]Aqueous solvents not statistically different due to high variability. [0]Polarity data not known for PBS. [1]Polarity based on the relative normalized E_T (30) $[E_T^N]$ polarity[41]

Solvent (excitation)	Relative polarity[1]	Stokes shift (nm)	Std dev.	Peak emission (RFU)	Std dev.
Isopropanol (337 nm)	0.546	77.1	0.7	889.1	13.4
n-Butyl alcohol (337 nm)	0.586	82.9	1.5	1135.3	70.4
Ethanol (334 nm)	0.654	92.1	0.2	1660.3	31.9
Methanol (333 nm)	0.762	98.1	0.3	2072.7	45.0
Water (330 nm)*[+]	1.000	110.9	1.70	1349.03	413.8
PBS (325 nm)[+]	—	118.3	0.6	2451.0	250.1

experiments based on solvent environment. This is supported by the similar, but not equivalent, findings of Meisner *et al.* which noted that the emissions of 1,2,3-triazoles were quenched in the polar-aprotic solvent dichloromethane compared to DMSO, which was attributed to the interruption of intra-molecular hydrogen bonds.[30] The authors described that the triazoles were acting as the hydrogen bond donor.[30] Conversely, the higher fluorescence (RFU > 800) in AT5 in polar protic solvents (Isopropanol, n-butyl alcohol, ethanol, methanol, PBS, and water), compared with very slight fluorescence (RFU < 30) in either polar aprotic solvents (DCM, toluene, ethyl-acetate, DMF, and DMSO) or aprotic solvents (acetone, chloroform, and cyclohexane) indicate that AT5 has increased fluorescence in solvents favoring AT5 behaving as a hydrogen bond acceptor (Fig. 5A and B and Table 1). In support of this as solvent polarity increases in protic solvents, there is a slight red-shift in emissions spectra ranging from 414.1 ± 0.702 nm (isopropanol) to 443.267 ± 0.643 nm (PBS) (Fig. 5C and D), though there is a less uniform red-shift as polarity increases in aprotic solvents as well (Fig. 5D). It is possible that the hydroxyl group present on C2″ could potentially form an intramolecular hydrogen bond with the ketone-group. Both the ketone-group and the amide group on C4′ can act as hydrogen bond acceptors, while the hydrogen ion on N2 of the triazole could potentially act as a hydrogen bond donor.

The strongest emissions of AT5 were observed in PBS, therefore subsequent experiments and characterization were performed in PBS. The absorbance spectra showed two major peaks, with the largest peak absorbance occurs between 262 and 263 nm (Fig. 5E). There was an additional smaller absorbance peak with a maximum occurring between 328 and 330 nm (Fig. 5E). The absorbance and emission intensity of both peaks was linked to concentration of AT5 (Fig. S5†). Excitation at 262 nm yielded slight emissions of 443.4 ± 40.99 RFU with a mean peak emission wavelength of 442 ± 2.8 nm (Fig. 5F). To determine which wavelength of excitation was ideal, the scanning excitation spectra (SES) for emissions at 442 nm, which systematically records the intensity of emissions at a given wavelength for each excitation wavelength, was recorded. Though excitation occurs at 262 nm, peak excitation for emissions at 442 nm most likely occurs at 324.7 ± 0.3 nm (Fig. 5F). This was confirmed by measuring emissions from AT5 excited

at 325 nm and found peak emissions at 443.3 ± 0.64 nm with peak emissions of 2451 ± 250.1 RFU (Fig. 5F). Because the highest absorbance peak did not correspond with peak fluorescence, the SES was used to determine peak excitation in all solvents. Using the peak SES and peak emissions (SE) to determine Stokes shift, a large Stokes shift of 118.3 ± 0.6 nm ($n = 3$) was observed for AT5 in PBS (Fig. 5F). Large Stokes shifts are a common feature of other triazoles.[29,30]

The SE Stokes shift of AT5 in various protic solvents (calculated as the difference in peak emissions, $n = 3$, compared to the peak excitation wavelength initially determined through SES) was observed to be linearly dependent on relative solvent polarity such that increasing polarity promotes a correlated increase in SE Stokes shift from 77.7 ± 0.7 nm in isopropanol to 118.36 ± 0.6 nm in PBS buffer (Table 1). The poor signal intensities presented in Fig. 5B for AT5 emissions in aprotic solvent systems introduce large error in estimation of the Stokes shift under these conditions. Indeed, the SE Stokes shift of AT5 in cyclohexane was determined to be 75.5 ± 27.5 nm, where the large standard deviation is likely due to low signal intensity with emissions of only 6.1 ± 5.9 RFU. Similar results were observed in all aprotic solvent systems examined. Moreover, identical experimental parameters (slit widths, integration times, *etc.*) were utilized for measurements collected in protic and aprotic solvent systems to allow for comparison of photophysical behaviors among all solvent systems examined. In contrast to aprotic conditions, protic conditions yield maximal AT5 emissions intensities, thereby allowing for estimation of SE Stokes shifts values with less than 2% experimental error (Table 1). The large SE Stokes shift of AT5 in PBS further indicates its potential as a useful biological probe.

Detergent micelle models

Since ionic detergents such as CTAB and sodium dodecyl-sulfate (SDS) have been shown to modulate the strength of fluorescent probes[20,45,46] and since detergent micelles have been used as membrane mimics for the study of membrane proteins,[47,48] it was decided that the interactions of AT5 with both ionic and neutral detergents should be characterized. To do this, various concentrations flanking the critical micelle concentration of CTAB, Triton X-100 (Triton), SDS, or Tween 20 (Tween) were separately mixed with 100 μM AT5 in PBS. For all
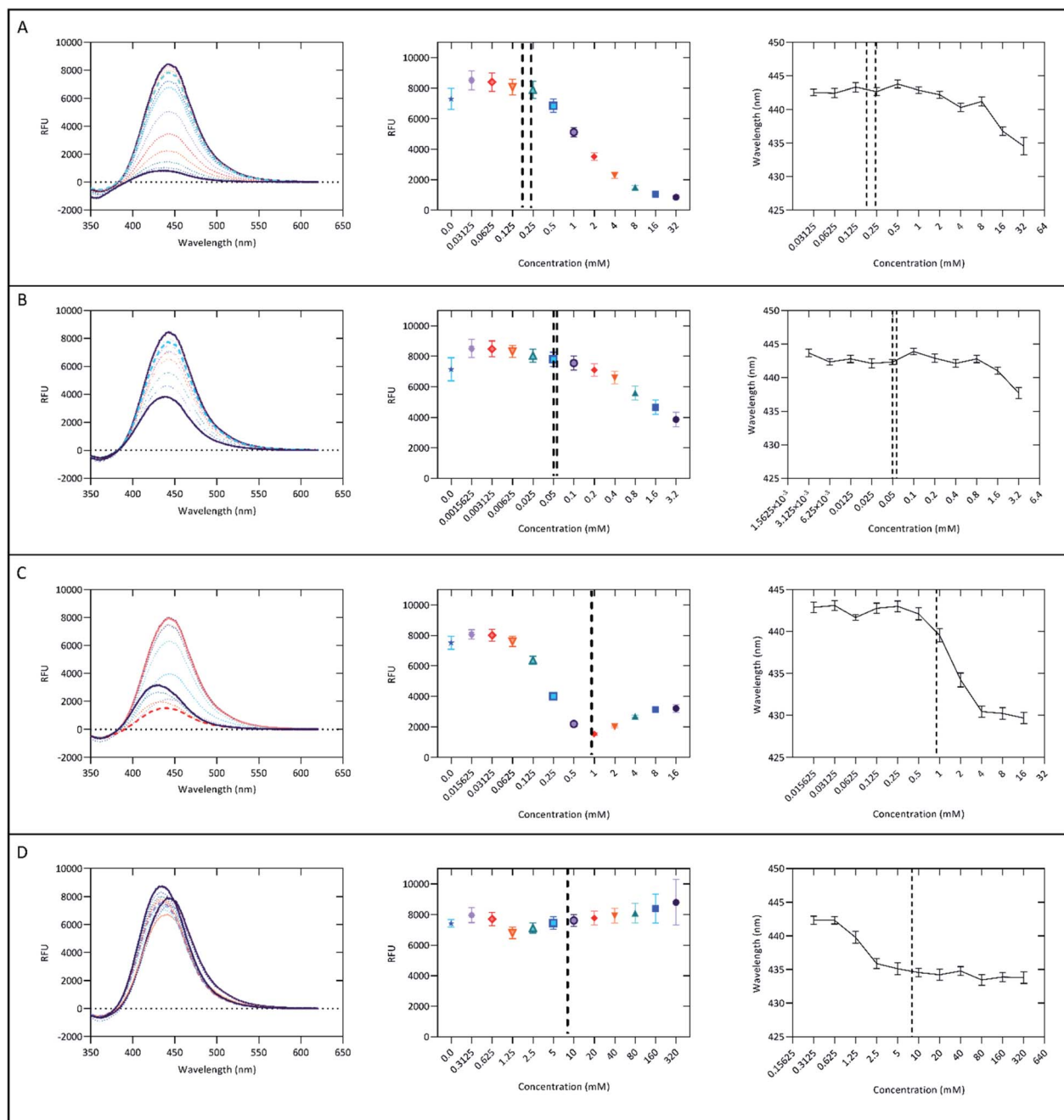
Fig. 6 Fluorescent properties of **AT5** in various detergents and PBS. Mean emissions spectra, mean peak emissions, and peak emissions wavelength of **AT5** in various concentrations of: (A) Triton X-100, (B) Tween 20, (C) CTAB, and (D) SDS. Dashed lines represent the CMC while two dashed lines represent the reported ranges of CMCs for each detergent. Column three displays the change in wavelength for each concentration at $\log_2$ intervals (Data at 0 mM not able to be shown). Each data is shown as the average of 9 wells from three, independent replicates $\pm$ SD (spectral standard deviation not shown).

detergents, the lowest concentration seemed to increase the fluorescence intensity of **AT5** (Fig. 6). As the concentration of both neutral detergents (Triton and Tween) increased, the emissions of **AT5** had an average percent decrease of 90.10 $\pm$ 0.73% and 54.72 $\pm$ 3.28%, respectively, demonstrating that neutral detergents had a strong quenching effect at concentrations above the CMC (Fig. 6A and B). Additionally, it was found that in 10 mM Triton X-100, addition of **AT5** prior to detergent

addition slightly increased fluorescence (Fig. S6†). Based on this, for all subsequent experiments, **AT5** was added prior to detergent. Unlike both neutral detergents, in the cationic detergent, CTAB, the emission of **AT5** was quenched at concentrations greater than 0.125 mM. For this condition, the average percent decrease was 80.8 $\pm$ 0.7% (of peak fluorescence at 0.03125 mM) with midpoint occurring at 0.25 mM CTAB (Fig. 6C). In SDS, the intensity of **AT5** was quenched at 1.25 mM
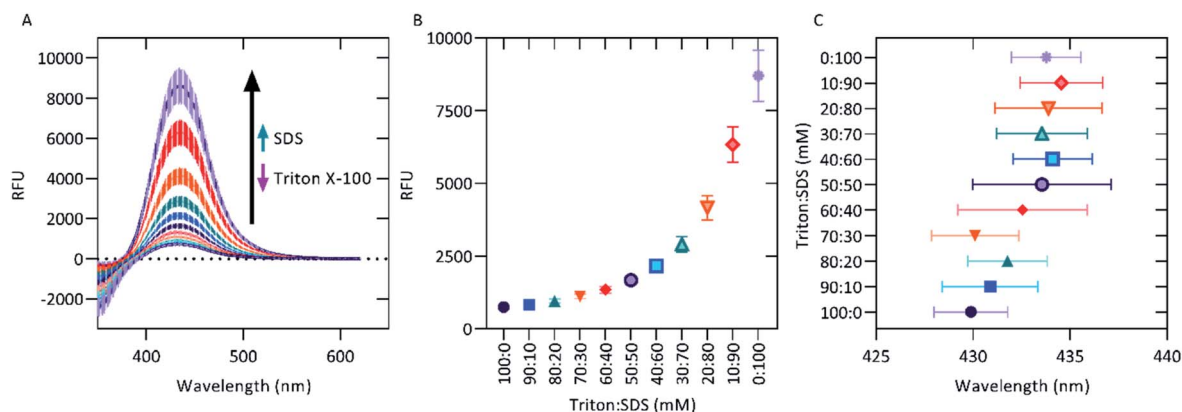
Fig. 7 Mixed micelles of varying concentrations of Triton X-100 and SDS. (A) Mean emissions spectra $\pm$ SD of 100 µM **AT5** in 100 mM of varying ratios of Triton X-100 to SDS in 1X PBS. The black arrow designates increase in SDS and a decrease in Triton. This is further illustrated by (B) the peak emission intensity $\pm$ SD for each ratio of detergent. The ratio shifts from 100 mM Triton X-100 and 0 mM SDS (left) to 0 mM Triton X-100 and 100 mM SDS (right). (C) Peak emission wavelength $\pm$ SD for each ratio of Triton X-100: SDS. Emissions were recorded using the CLARIOstar microplate reader on a 96-well UV : vis microplate in triplicate for three, independent replicates ($n = 9$).

to approximately 14.7 $\pm$ 1.1% lower than its initial peak fluorescence (at 0.3125 mM, Fig. 6D). In all detergents as concentrations increased, there was a slight but noticeable blue-shift in peak emissions wavelength, with the most drastic change occurring in CTAB shifting from a peak emission wavelength around 443 nm (all concentrations < 0.25 mM) to a peak emissions wavelength around 430 nm (all concentrations > 4 mM) (Fig. 6C).

Due to the quenching effect of Triton and the lack of quenching observed with higher concentrations of SDS, we decided to use these detergents to mimic a mixed lipid composition environment. We hypothesized that, as the molar ratio shifted from a large Triton concentration to a large SDS concentration, we would observe increasing emission intensities. Indeed, a broad range of emission intensities from 100 µM **AT5** from 753.4 $\pm$ 49.5 RFUs (100 mM Triton: 0 mM SDS) to 8705 $\pm$ 872 RFUs (0 mM Triton: 100 mM SDS) (Fig. 7A and B). This implies that in regions of anionic lipids (as opposed to neutral lipids), **AT5** would have increased fluorescence. Peak emission wavelengths were also shown to slightly shift as the detergent concentration shifted from Triton to SDS (Fig. 7C), matching those observed in high concentrations of Triton and SDS (Fig. 6A, D, 7C). Ionic detergents such as CTAB and SDS can affect fluorescence through their ability to form, or disrupt, hydrogen bonds.[49,50] These data potentially indicate a possible interruption of the hydrogen bonding of water to **AT5**. It is also possible for ionic interactions between the anionic head group of SDS with the amide nitrogen of **AT5** on its side chain leading to an effect the fluorescent properties of **AT5**, while the blue-shift observed in all detergents may be due to increasing hydrophobic interactions.[51]

Conclusions

Aurones are a widely researched class of flavonoid with many bioactivities. Recently there has been increased interest in their use as fluorescent probes. "Click" 1,2,3-triazole structures have

also been shown to have potential use as fluorophores as well. Recently, our group has synthesized and characterized aurone-derived triazoles. Five of these aurone-derived triazoles (**AT1–5**) were examined for their potential use as live-cell fluorescent probes. Of these five, **AT2** and **AT5** fluoresced in cells, but **AT5** was the only compound which was not substantially cytotoxic, potentially due to its R' group. **AT5** was shown to have high fluorescence intensity in polar protic solvents, potentially implying the need for **AT5** to act as a hydrogen bond acceptor, though further study is warranted. In micellular models, emissions of **AT5** were quenched in detergents at most concentrations below the CMC, though the fluorescence recovery observed in ionic detergents indicates the potential for ionic interactions with **AT5**, and their potential effect on the fluorescent properties of **AT5**. Here **AT5** was shown to have potential as a fluorophore in live-cell microscopy.

Author contributions

Daniel L. Bryant: conceptualization, data curation, formal analysis, investigation, project administration, validation, visualization, and writing - original draft. Arjun Kafle: conceptualization, data curation, formal analysis, methodology, resources, and writing – original draft. Anthony L. Farone: funding acquisition, supervision, and writing – review & editing. Scott T. Handy: conceptualization, funding acquisition, supervision, and writing – review & editing. Justin M. Miller: conceptualization, funding acquisition, project administration, supervision, visualization, and writing – review and editing.

Conflicts of interest

There are no conflicts to declare.

Acknowledgements

Notes and references

1 S. Asen, K. H. Norris and R. N. Stewart, *Phytochemistry*, 1972, **11**, 2739–2741.

2 G. Sui, T. Li, B. Zhang, R. Wang, H. Hao and W. Zhou, *Bioorg. Med. Chem.*, 2021, **29**, 115895.

3 H. S. Park, D. E. Nelson, Z. E. Taylor, J. B. Hayes, K. D. Cunningham, B. A. Arivett, R. Ghosh, L. C. Wolf, K. M. Taylor, M. B. Farone, S. T. Handy and A. L. Farone, *Int. Immunopharmacol.*, 2017, **43**, 116–128.

4 S. Y. Shin, M. C. Shin, J.-S. Shin, K.-T. Lee and Y. S. Lee, *Bioorg. Med. Chem. Lett.*, 2011, **21**, 4520–4523.

5 B. P. Bandgar, S. A. Patil, B. L. Korbad, S. C. Biradar, S. N. Nile and C. N. Khobragade, *Eur. J. Med. Chem.*, 2010, **45**, 3223–3227.

6 M.-Y. Song, G.-S. Jeong, H.-S. Lee, K.-S. Kwon, S.-M. Lee, J.-W. Park, Y.-C. Kim and B.-H. Park, *Biochem. Biophys. Res. Commun.*, 2010, **400**, 83–88.

7 F. M. Alqahtani, B. A. Arivett, Z. E. Taylor, S. T. Handy, A. L. Farone and M. B. Farone, *PLOS ONE*, 2019, **14**, e0226068.

8 O. Kayser, A. F. Kiderlen and R. Brun, *Planta Med.*, 2001, **67**, 718–721.

9 G. Alsaif, N. Almosnid, I. Hawkins, Z. Taylor, D. L. T. Knott, S. Handy, E. Altman and Y. Gao, *Curr. Pharm. Biotechnol.*, 2017, **18**, 384–390.

10 R. Václavíková, E. Kondrová, M. Ehrlichová, A. Boumendjel, J. Kovář, P. Stopka, P. Souček and I. Gut, *Bioorg. Med. Chem.*, 2008, **16**, 2034–2042.

11 N. J. Lawrence, D. Rennison, A. T. McGown and J. A. Hadfield, *Bioorg. Med. Chem. Lett.*, 2003, **13**, 3759–3763.

12 N. Shanker, O. Dilek, K. Mukherjee, D. W. McGee and S. L. Bane, *J. Fluoresc.*, 2011, **21**, 2173–2184.

13 C. Espinosa-Bustos, D. Cortés-Arriagada, M. A. Soto-Arriaza, J. Robinson-Duggon, N. Pizarro, A. R. Cabrera, D. Fuentealba and C. O. Salas, *Photochem. Photobiol. Sci.*, 2017, **16**, 1268–1276.

14 Y. Xue, Y. Dou, L. An, Y. Zheng, L. Zhang and Y. Liu, *RSC Adv.*, 2016, **6**, 7002–7010.

15 K. Muñoz-Becerra, N. Villegas-Escobar, C. Zúñiga-Loyola, D. Cortés-Arriagada and A. Toro-Labbé, *Mol. Phys.*, 2019, **117**, 1451–1458.

16 H. Chen, Y. Sun, C. Zhou, D. Cao, Z. Liu and L. Ma, *Spectrochim. Acta, Part A*, 2013, **116**, 389–393.

17 H. Chen, Z. Liu, D. Cao, S. Lu, J. Pang and Y. Sun, *Sens. Actuators, B*, 2014, **199**, 115–120.

18 Y. Xu, H. Chen, R. Guan, D. Cao, Q. Wu and X. Yu, *Fibers Polym.*, 2016, **17**, 181–185.

19 M. Zhang, Y.-T. Bao, W. Yang, H.-F. Xiao, Z.-X. Han, X. Wu and L. Yang, *J. Heterocycl. Chem.*, 2018, **55**, 1130–1135.

20 A. Kafle, S. Bhattarai, J. M. Miller and S. T. Handy, *RSC Adv.*, 2020, **10**, 45180–45188.

21 T. A. Geissman and J. B. Harborne, *J. Am. Chem. Soc.*, 1955, **77**, 4622–4624.

22 R. S. Varma and M. Varma, *Tetrahedron Lett.*, 1992, **33**, 5937–5940.

23 X. Qi, R. Li and X.-F. Wu, *RSC Adv.*, 2016, **6**, 62810–62813.

24 T.-T. Jong and S.-J. Leu, *J. Chem. Soc., Perkin Trans. 1*, 1990, 423–424, DOI: **10.1039/P19900000423**.

25 H. Harkat, A. Blanc, J.-M. Weibel and P. Pale, *J. Org. Chem.*, 2008, **73**, 1620–1623.

26 I. Hawkins and S. T. Handy, *Tetrahedron*, 2013, **69**, 9200–9204.

27 A. Kafle, S. Bhattarai and S. T. Handy, *Synthesis*, 2020, **52**, 2337–2346.

28 D. Ghosh, S. Rhodes, K. Hawkins, D. Winder, A. Atkinson, W. Ming, C. Padgett, J. Orvis, K. Aiken and S. Landge, *New J. Chem.*, 2015, **39**, 295–303.

29 Y.-C. Zhang, R. Jin, L.-Y. Li, Z. Chen and L.-M. Fu, *Molecules*, 2017, **22**, 1380.

30 Q. J. Meisner, J. V. Accardo, G. Hu, R. J. Clark, D.-e. Jiang and L. Zhu, *J. Phys. Chem. A*, 2018, **122**, 2956–2973.

31 H. E. Gottlieb, V. Kotlyar and A. Nudelman, *J. Org. Chem.*, 1997, **62**, 7512–7515.

32 J. Schindelin, I. Arganda-Carreras, E. Frise, V. Kaynig, M. Longair, T. Pietzsch, S. Preibisch, C. Rueden, S. Saalfeld, B. Schmid, J.-Y. Tinevez, D. J. White, V. Hartenstein, K. Eliceiri, P. Tomancak and A. Cardona, *Nat. Methods*, 2012, **9**, 676–682.

33 W. Li, M. Zhang, J. Zhang and Y. Han, *Front. Chem.*, 2006, **1**, 438–442.

34 Y. Moroi, K. Motomura and R. Matuura, *J. Colloid Interface Sci.*, 1974, **46**, 111–117.

35 B. Hammouda, *J. Res. Natl. Inst. Stand. Technol.*, 2013, **118**, 151–167.

36 K. Kalyanasundaram and J. K. Thomas, *J. Am. Chem. Soc.*, 1977, **99**, 2039–2044.

37 S. K. Hait and S. P. Moulik, *J. Surfactants Deterg.*, 2001, **4**, 303–309.

38 D. Koley and A. J. Bard, *Proc. Natl. Acad. Sci. U. S. A.*, 2010, **107**, 16783–16787.

39 G. E. Tiller, T. J. Mueller, M. E. Dockter and W. G. Struve, *Anal. Biochem.*, 1984, **141**, 262–266.

40 A. Patist, S. S. Bhagwat, K. W. Penfield, P. Aikens and D. O. Shah, *J. Surfactants Deterg.*, 2000, **3**, 53–58.

41 C. Reichardt and T. Welton, in *Solvents and Solvent Effects in Organic Chemistry*, Ed. C. Reichardt and T. Welton, 2010425–508, 549–586, DOI: DOI: **10.1002/9783527632220**.

42 C. Reichardt, *Chem. Rev.*, 1994, **94**, 2319–2358.

43 M. J. Kamlet, J. L. Abboud and R. W. Taft, *J. Am. Chem. Soc.*, 1977, **99**, 6027–6038.

44 Y. Marcus, *The Properties of Solvents*, John Wiley & Sons Ltd, West Sussex, England, 1998.

45 H. Tian, J. Qian, H. Bai, Q. Sun, L. Zhang and W. Zhang, *Anal. Chim. Acta*, 2013, **768**, 136–142.

46 D. Tai and J. Liu, *Luminescence*, 2015, **30**, 358–361.

47 R. M. Garavito and S. Ferguson-Miller, *J. Biol. Chem.*, 2001, **276**, 32403–32406.

48 A. M. Seddon, P. Curnow and P. J. Booth, *Biochim. Biophys. Acta, Rev. Biomembr.*, 2004, **1666**, 105–117.

49 O. S. Nnyigide, S.-G. Lee and K. Hyun, *Sci. Rep.*, 2019, **9**, 10643.

50 S. Javadian, V. Ruhi, A. Heydari, A. Asadzadeh Shahir, A. Yousefi and J. Akbari, *Ind. Eng. Chem. Res.*, 2013, **52**, 4517–4526.

51 H. Li, T.-Z. Xie, Z. Liang, D. Dahal, Y. Shen, X. Sun, Y. Yang, Y. Pang and T. Liu, *Chem. Commun.*, 2019, **55**, 330–333.